$Mn^+(H_2)_n$ and $Zn^+(H_2)_n$ Clusters: Influence of 3d and 4s Orbitals on Metal−Ligand Bonding

Patrick Weis, Paul R. Kemper, and Michael T. Bowers*

Department of Chemistry, University of California at Santa Barbara, Santa Barbara, California 93106-9510

Received: December 3, 1996; In Final Form: February 7, 1997[⊗]

Equilibrium methods were used to measure ΔG_T° as a function of temperature for the sequential clustering of up to six H_2 ligands to the $Mn^+(3d^54s^1\ ^7S)$ and $Zn^+(3d^{10}4s^1\ ^2S)$ core ions. The resulting binding energies are by far the lowest in the first-row transition metal series, ranging from 3.75 kcal/mol for $Zn^+(H_2)$ and 1.9 for $Mn^+(H_2)$ down to 1−1.5 kcal/mol for the highly ligated clusters. Density functional theory calculations using the B3-LYP parametrization were performed to provide information on structures, vibrational frequencies, and orbital populations, which, together with the experimental data, give insight into the types of bonding that are present. It was found that the repulsion between the singly occupied 4s orbital and the H_2 σ orbital accounts for the low binding energies and that the 4p orbitals play a key role in reducing this repulsion.

Introduction

Transition metals play a key role in a vast number of catalytic reactions—from biological systems to industrial processes. The common feature in all these reactions is the ability of the transition metal to activate σ bonds. Despite their widespread usage, many details of these reactions are still not well understood and are still the object of significant experimental and theoretical interest. In recent years we have tried to shed some light on the elementary steps of the catalytic reactions by examining simple, prototypic systems such as the interaction of gas phase metal ions with dihydrogen[1−9] and methane.[9,10] These $M^+(H_2)_n$ and $M^+(CH_4)_n$ clusters are small enough to allow modeling with the high-level ab initio electronic structure calculations that have proven to be necessary for a thorough understanding of the underlying processes.[11] We have obtained accurate thermodynamic data for the dihydrogen complexes of Sc^+, Ti^+, V^+, Cr^+, Fe^+, Co^+,[1−6] and, very recently, Ni^+ [7]and Cu^+ [8] with up to six H_2 ligands attached. Despite the apparent similarity of these $M^+(H_2)_n$ systems, there is a great diversity in the strength of the M−H_2 interaction as measured bond dissociation energies (BDE's) range from ∼2.4 kcal/mol for $Sc^+(H_2)$ to more than 21 kcal/mol for triplet $V^+(H_2)_{1-4}$. Furthermore, the maximum first solvation shell coordination number ranges from 4 (Cu^+) to 5 (Ni^+) to 6 (Ti^+, Cr^+, Fe^+, and Co^+). Fundamentally different types of bonding are also found, including ligand-induced spin changes (Fe^+H_2[5] and $V^+(H_2)_6$[3]) and H−H bond insertion (Sc^+H_2[1]).

Theoretical investigations[11] have pointed out four major effects that influence the bonding in these ions: electrostatic charge-induced dipole and charge quadrupole attractions; the presence or absence of Pauli repulsion along the bond axis which is in turn influenced by 3d/4s and 3d/4s/4p hybridization;[11,12] donation from the H_2 ligands into the metal σ orbitals (primarily the 4s but also the 3dσ);[11,13,14,15] and finally, back-donation from the M^+ 3dπ orbitals into the H_2 σ^* orbital.[14,15] As a consequence, the M^+-H_2 interaction is very sensitive to the metal's valence electron structure. The aforementioned metal ions either start with an empty 4s orbital, i.e., a $3d^n4s^0$ configuration (V^+, Cr^+, Co^+, Ni^+, Cu^+), or are promoted to this configuration upon ligation of the first H_2 (Ti^+, Fe^+). In the present paper, we investigate the effect of forced occupation of the 4s orbital by studying the bonding between H_2 and the $Zn^+(3d^{10}4s^1)$ and $Mn^+(3d^54s^1)$ ions. For Zn^+, the 3d shell is already full while for Mn^+ promotion to the lowest $3d^6$ configuration requires too much energy to occur (41 kcal/mol[16]). Hence, the 4s orbital must remain occupied.

Systematic studies of the kind done for metal ions interacting with dihydrogen are very difficult to do in neutral systems. In fact, the first solution phase dihydrogen complex of any kind was not reported until 1984,[17] and no studies are available for bare neutral first-row transition metal atoms. These neutral metal atoms are also completely unreactive with alkanes and only weakly reactive with alkenes.[18] The reason is that all first-row transition metals have the $4s^23dn^{-2}$ configuration except for $Cr(4s^13d^5)$ and $Cu(4s^13d^{10})$. Since the 4s orbital is much larger than the 3d orbital for most of the first-row metals,[19] the dominant reaction is repulsive with coordinately saturated systems like H_2 and alkanes due to the Pauli exclusion principle. Only when strongly oxidizing ligands, such as cyclopentyldienyl radical (Cp), are added to the metal center does it become activated, or "metal ion like". This tuning of the metal center activity by selective ligand attachment is a central feature of transition metal chemistry in solution.

In the gas phase we expect the presence of even a single 4s electron to destabilize the M^+-H_2 bond due to the additional Pauli repulsion. By studing the equilibrium clustering of these ions, however, we can determine quantitatively how large the destabilization is. Further, our theoretical investigation can identify the polarization/hybridization in the cluster which reduces this repulsion. Of particular interest is the extent of involvement of the 4p orbitals. Despite their high energy (105 and 138 kcal/mol above the ground state for Mn^+ and Zn^+, respectively[16]), these orbitals have been invoked to explain the geometries of $Co^+(H_2)_{3,4}$[14] and $Fe^+(H_2)_{3,4}$.[5] We also hope to better understand the influence of a filled or half-filled 3d shell on the bonding. With these goals in mind, this paper compares the H_2 ligation behavior (BDE's, geometries, orbital populations) of Mn^+ and Zn^+ with each other ($3d^54s^1$ vs $3d^{10}4s^1$) and with the metals preceding them in the periodic table, chromium and copper, that have cationic ground states with the same d-shell occupation but an *empty* 4s orbital (Cr^+: ^6S $3d^5$, Cu^+: ^1S $3d^{10}$).

Experimental Section

A detailed description of the apparatus and the evaluation procedure has been given elsewhere;[4,20] therefore, only a short

[⊗] Abstract published in *Advance ACS Abstracts,* March 15, 1997.

S1089-5639(96)03963-1 CCC: $14.00

summary will be presented here. The metal cations are formed by a glow discharge in neon (1−5 Torr) with a zinc (manganese) cathode at typically 500−1000 V negative with respect to the body of the ion source. The ions leave the source through a 2 mm diameter hole, are mass selected in a first quadrupole mass spectrometer, and injected into a drift cell (length 4 cm, entrance and exit orifices with 0.15 mm diameter) filled with hydrogen at a pressure of typically 3 Torr (monitored with an accuracy of 1% with a capacitance manometer[21]). In the cell, the metal ions react with H_2, forming an equilibrium distribution of the different metal−hydrogen clusters, $M^+(H_2)_n$. Their relative abundances are mass analyzed with a second quadrupole mass spectrometer after the drift cell and detected with a conversion dynode/electron multiplier. The resulting ion counts are collected with a synchronously scanned multichannel scaler.[22] The integrated intensities ($M^+(H_2)_n$ and $M^+(H_2)_{n-1}$), together with the H_2 pressure in Torr (P_{H_2}), allow us to determine the equilibrium constant K_{eq} and free energy of association ΔG_T° as a function of temperature (T, in K) using the standard methods of thermodynamics:

$$K_{eq} = \frac{[Cr^+(H_2)_n]\cdot 760}{[Cr^+(H_2)_{n-1}]P_{H_2}} \quad (1)$$

$$\Delta G_T^\circ = -RT \ln K_{eq} \quad (2)$$

The slope of the experimental ΔG_T° vs T plot gives the experimental ΔS_T° and the intercept ΔH_T°. While the ΔH_T° values might appear to be the more useful, entropy measurements can provide important clues to the actual clustering processes which occur.

Control experiments performed at different pressures (in the range between 0.5 and 5 Torr) showed no significant pressure dependence of K_{eq}, i.e., that the measured abundances do reflect the equilibrium distribution. Higher cell pressures are technically possible (up to 50 Torr), but for the very weakly bound clusters investigated here such high pressures lead to an increase in collision-induced dissociation near the cell exit and were thus not utilized. In the case of zinc most measurements were performed with ^{68}Zn. Control experiments with ^{64}Zn and ^{66}Zn showed no isotope dependence.

In the experiments presented in this paper, the cell temperature was varied between 77 and 400 K. In order to obtain the bond dissociation energies (BDE's $= -\Delta H_0^\circ = -\Delta G_0^\circ$), the free energy ΔG_T° was extrapolated to 0 K. This was done with a fitting procedure that calculates ΔG_T° as a function of the translational, rotational, and vibrational sums of states. The exact calculation of ΔG_T° by means of statistical thermodynamics is in principle straightforward but requires a detailed knowledge of both the molecule's vibrations (including anharmonicities, especially for the low-frequency vibrations) and its geometry. While the geometries of these fairly small ions are well described at even moderate levels of theory,[11] the vibrational frequencies and anharmonicities can be calculated only to a limited accuracy. The lowest frequecies are especially problematic since they correspond to essentially free internal rotations of the H_2 ligands. Treating these high-energy rotations as very low-frequency vibrations causes serious errors in the calculated association entropies. We therefore scaled the calculated frequencies to reproduce the measured slope of the ΔG_T° vs T line. (An alternative procedure would be to treat some of the low-frequency vibrations explicitly as internal rotations; however, this is complicated by both the interaction of the internal and molecular rotations and the ortho/para effects in the H_2 ligands.) Note that the somewhat ambiguous frequency scaling factor only affects the slope, but not the intercept of the ΔG_T° curve, and hence does not affect binding energies. For a thorough discussion of the fitting procedure and an estimation of the errors involved, see refs 1and 4.

Using electronic state chromatography (ESC),[23] we were able to probe the metal ion electronic state distribution. It is difficult to get a precise measurement of the fraction of excited state since it is partially deactivated by the He bath gas in the ESC experiment. Our measurements indicate for Mn^+ there was about 90−95% ground state ^7S ($3d^54s^1$) and 5−10% excited states ($3d^64s^0$). These excited state ions react with H_2 to form MnH^+, a reaction that is endothermic for ground state ions. These MnH^+ ions subsequently cluster to form a series of $MnH^+(H_2)_n$ ion which were also investigated in these experiments. No excited state Zn^+ ions were observed, and ground state Zn^+ did not react to form ZnH^+.

Theoretical Methods

The association enthalpies and entropies are the only cluster properties measured in our experiment. Molecular parameters such as geometries, orbital populations, and vibrational frequencies are calculated with the density functional theory (DFT) method,[24,25] utilizing Becke's "B3LYP" functional.[26−29] These parameters together with the experimental ΔG_T° measurements allow us to determine the BDE's (ΔH_0°) values for the individual clusters. The comparison of measured and calculated BDE's connects theory and experiment and allows us to judge the quality of the theoretical method for these systems. The B3LYP parametrization has been successfully applied by both our group and others to a variety of first-row transition metal M^+-H_2 clusters, such as $Co^+(H_2)_n$,[14] $Cr^+(H_2)_n$,[4] $Cu^+(H_2)_n$,[8,30] and $Ti^+(H_2)_n$.[2] The calculations were performed on a IBM RISC 6000 workstation using TURBOMOLE[32,33] (geometry optimizations, electron density plots) and GAUSSIAN 94[34] (frequencies and natural bond analysis). TURBOMOLE's split valence + polarization function (SVP) basis set[35] was used throughout. The polarization function exponents were 0.128 (Mn), 0.162 (Zn), and 0.8 (H). The zinc frequencies are calculated for the average atomic mass of the natural isotope distribution. The frequencies are essentially independent of the isotope.

Results and Discussion

The experimental results for Mn^+ and $Zn^+$are shown in Figures 1 and 2. Binding energies (experimental and theoretical) are summarized in Table 1 and the theoretical geometries in Figures 3 and 4. The corresponding Mn^+ and Zn^+ clusters are discussed together.

Mn^+H_2 and Zn^+H_2. The equilibrium for the binding of the first H_2 molecule was followed from 300 to 77 K with Mn^+ and from 300 to 110 K with Zn^+. The experimental ΔH_T° and ΔS_T° values for Zn^+were −4.25 kcal/mol and −14.4 cal/(mol K) (Table 1); the corresponding results for Mn^+ were −2.4 kcal/mol and −13.1 cal/(mol K). Figures 1 and 2 show both the experimental free energies (points) and those calculated from statistical thermodynamics using the theoretically calculated frequencies and moments of inertia (lines). In order to reproduce the experimental slope ($=\Delta S_T^\circ$), we had to scale the low-frequency modes (those below 500 cm^{-1}) by 0.9 in the case of Mn^+H_2 and by 0.7 in the case of Zn^+H_2. This leaves the axis intercept (i.e., $-\Delta H_T^\circ$) as the only variable. We find bond dissociation energies of 1.9 kcal/mol for Mn^+-H_2, and 3.75 kcal/mol for Zn^+-H_2 (Table 1). The calculated (DFT) binding energies for Mn^+H_2 and Zn^+H_2 are 2.54 and 4.94 kcal/mol,

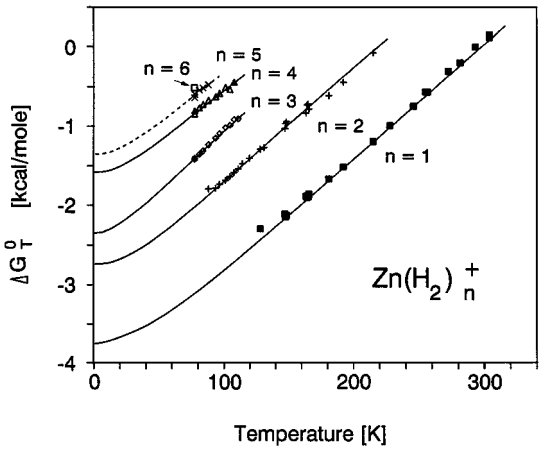

Figure 1. Plot of the experimental free energy, ΔG°_T, versus temperature for the reaction: $Zn^+(H_2)_{n-1} + H_2 \rightleftarrows Zn^+(H_2)_n$ for $n = 1$ to 6. The solid lines are fits using statistical mechanics (see text). The intercepts give the standard heat of formation, ΔH°_0 (= −bond dissociation energy, BDE); the slopes give the standard entropy of association (ΔS°_T). For $n = 5$ and 6 the experimental data range is not sufficent for a unequivocal fit of the slope of ΔG°_T; therefore, the free energy function for the fourth cluster is shifted to match the experimental data (dashed line).

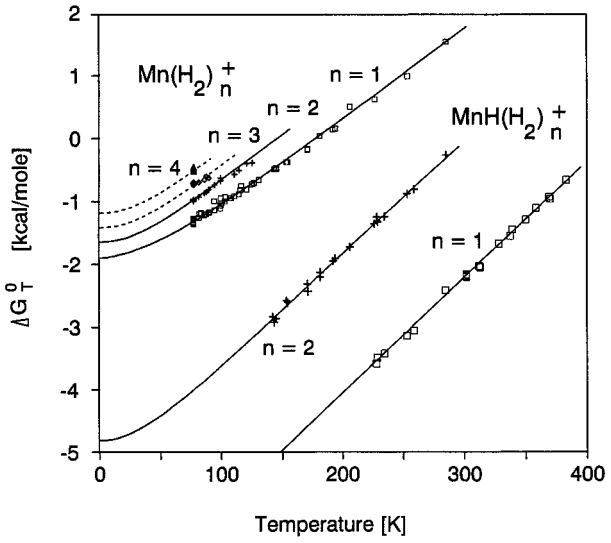

Figure 2. Plot of the experimental free energy, ΔG°_T, versus temperature for the reaction $Mn^+(H_2)_{n-1} + H_2 \rightleftarrows Mn^+(H_2)_n$ for $n = 1-4$ and for the reaction $MnH^+(H_2)_{n-1} + H_2 \rightleftarrows MnH^+(H_2)_n$ for $n = 1$ and 2. The solid lines are fits using statistical mechanics (see text). The intercepts give the standard heat of formation, ΔH°_0 (= −bond dissociation energy, BDE). For the third and forth $Mn^+(H_2)_n$ cluster the experimental data range is not sufficent for a unequivocal fit of the slope of ΔG°_T, and the free energy function for the second cluster is shifted to match the experimental data (dashed lines).

respectively (Table 1). Although this is an overestimation of about 25%, the agreement is reasonable considering the small energies involved. The calculated metal−hydrogen distances are 2.54 Å for Mn^+H_2 and 2.27 Å for Zn^+H_2; the corresponding H−H distances are 0.768 and 0.774 Å (Figures 3 and 4).

These metals have the smallest first ligand binding energies and entropies of any first-row transition metal M^+H_2 cluster.[1−8] They are comparable with the purely electrostatic interaction in K^+H_2, which has a BDE of only 1.45 kcal/mol.[36] In contrast, Cu^+H_2 ($3d^{10}$) is bound by 15.4 kcal/mol[8] while Cr^+H_2 ($3d^5$) is bound by 7.6 kcal/mol,[4] both 4 times stronger than the 4s electron containing Zn^+H_2 and Mn^+H_2 ions. The corresponding Cu^+H_2 and Cr^+H_2 association entropies are also larger (−19.7 and −17.0 cal/(mol K), respectively), further illustrating the more tightly bound nature of these ions.

TABLE 1: Experimental and Calculated Bond Dissociation Energies and Entropies

	theory		experiment	
	D_e[a]	D_0[a]	$-\Delta H^\circ_0$[a]	$-\Delta S^\circ_T$[b]
$Mn^+(H_2)$	3.41	2.54	1.90 ± 0.4	13.1 ± 2
$Mn^+(H_2)_2$	3.02	1.56	1.65 ± 0.4	11.7 ± 2
$Mn^+(H_2)_3$	2.80	1.30	(1.4)[c]	
$Mn^+(H_2)_4$	1.84	0.82	(1.2)[c]	
$MnH^+(H_2)$	9.17	7.26	7.15 ± 0.5	18.0 ± 2
$MnH^+(H_2)_2$	6.96	4.74	4.80 ± 0.5	17.6 ± 2
$Zn^+(H_2)$	6.06	4.94	3.75 ± 0.4	14.4 ± 2
$Zn^+(H_2)_2$	4.47	3.10	2.75 ± 0.4	14.2 ± 2
$Zn^+(H_2)_3$	3.64	2.17	2.35 ± 0.4	15.2 ± 2
$Zn^+(H_2)_4$	2.25	1.20	1.60 ± 0.4	12.6 ± 2
$Zn^+(H_2)_5$	1.76	1.12	1.50 ± 0.4	13.5 ± 2
$Zn^+(H_2)_6$	1.83	1.22	(1.4)[c]	
$Cr^+(H_2)$[d]	9.84	8.36	7.6 ± 0.5	17.0 ± 2
$Cu^+(H_2)$[e]	17.88	16.03	15.4 ± 0.5	19.7 ± 2

[a] In kcal/mol. [b] In cal/(mol K). [c] Insufficient temperature range to determine ΔS°_T; ΔG°_T, curve from previous cluster shifted to match points. See text. [d] From ref 4. [e] From ref 8.

The addition of a 4s electron acts to reduce the M^+-H_2 bond strength in several ways. The first is the increase in Pauli repulsion along the bond axis. This increased repulsion is much more important than that caused by 3dσ occupation in Cr^+ and Cu^+ due to the much larger size of the 4s orbital. As a consequence, the Zn^+-H_2 and Mn^+-H_2 bond lengths are more than 0.5 Å longer than those in Cu^+H_2 (1.71 Å)[8,30] and Cr^+H_2 (2.00 Å).[4]

Second, σ donation from H_2 to the metal ion is greatly reduced for two reasons: (1) the overlap between the M^+ 4s and the H_2 σ orbitals is smaller due to the greater metal−hydrogen bond lengths, and (2) the presence of an electron in the 4s orbital directly inhibits donation into that orbital (the 4s normally receives most of the σ donation).[11] Because the orbital already contains one electron (of α spin), it can accept only β-spin density. This forces the H_2 ligands either to have some unpaired spin or to transfer electron density of α-spin into the energetically unfavorable metal 4p orbital. The natural bond orbital (NBO) populations[37] (Table 2) show that the amount of σ donation is reduced with respect to that in Cr^+H_2 and Cu^+H_2.

Third, the longer metal−hydrogen bond lengths also reduce the amount of back-donation from the 3dπ orbitals into the H_2 σ^* orbital as shown in the NBO populations (Table 2). The 3d populations in Mn^+H_2 and Zn^+H_2 are essentially unchanged compared to the bare metal ion, indicating that no significant M^+3d to H_2 σ^* back-donation occurs. In Cu^+H_2 and Cr^+H_2, on the other hand, the 3d orbital occupation is decreased significantly (Table 2), showing the presence of back-bonding in these ions. This difference in back-donation can also be seen in the H−H vibrational frequencies and bond lengths. In Mn^+H_2 (Zn^+H_2), the calculated H−H stretch frequency is only 107 cm^{-1} (193 cm^{-1}) lower than the calculated H−H vibration in the H_2 molecule. In Cr^+H_2 and Cu^+H_2, on the other hand, this frequency is lowered by 347 and 569 cm^{-1}, respectively, due to back-donation into the H_2 σ^* orbital. The H−H bond distance is also longer in Cr^+H_2 and Cu^+H_2 for the same reason. Based on comparison of early and late transition metal M^+H_2 complexes, the absence of back-bonding in Zn^+H_2 reduces the BDE by about 6 kcal/mol. The effect on Mn^+H_2 is almost certainly smaller but hard to estimate. The sum of the three effects discussed here results in a large reduction in the BDE's which we observe, as well as more positive association entropies

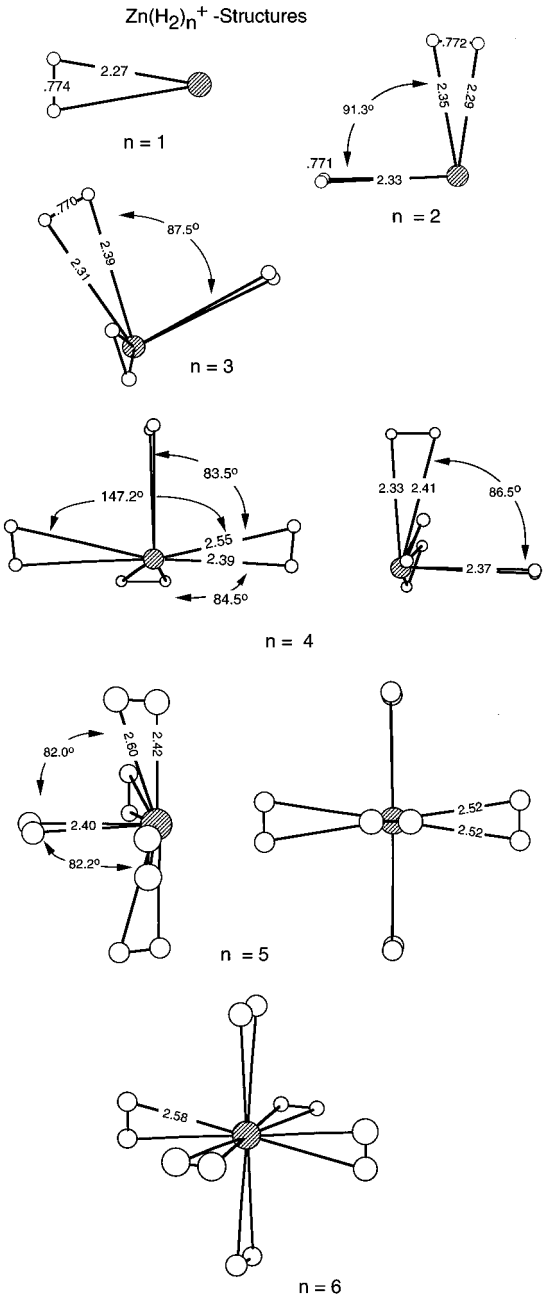

Figure 3. Calculated structures for $Zn^+(H_2)_n$, for $n = 1-6$; see text for details on method. All distances are in angstroms. The calculated H−H distance is 0.767 ± 0.001 Å. In (a) and (b), for $n = 4$ and $n = 5$, the two structures are related by a 90° rotation around the vertial axis in the plane of the paper.

due to the longer M^+-H_2 bond length and the reduction in M^+-H_2 vibrational frequencies (all relative to those in Cu^+H_2 and Cr^+H_2).

This repulsion by the 4s electron is hardly surprising. Perhaps more interesting are the variety of ways in which the ion attempts to mitigate these destabilizing effects. The data in Table 2 and Figure 5 indicate both Mn^+ and Zn^+ make use of a 4p orbital to polarize the 4s orbital. The differential population contours in Figure 5 show the electron density on Zn^+ is moved opposite the H_2 ligand, thereby reducing the repulsion due to the Pauli exclusion effect. This electron density increase opposite the H_2 ligand is due to partial hybridization of the 4s orbital with the $4p_z$ orbital forming two sp hybrid orbitals. The one pointed away from the H_2 ligand takes some of the original 4s electron density, while the empty orbital oriented toward the H_2 ligand accepts electron density from the H_2 σ orbital. The

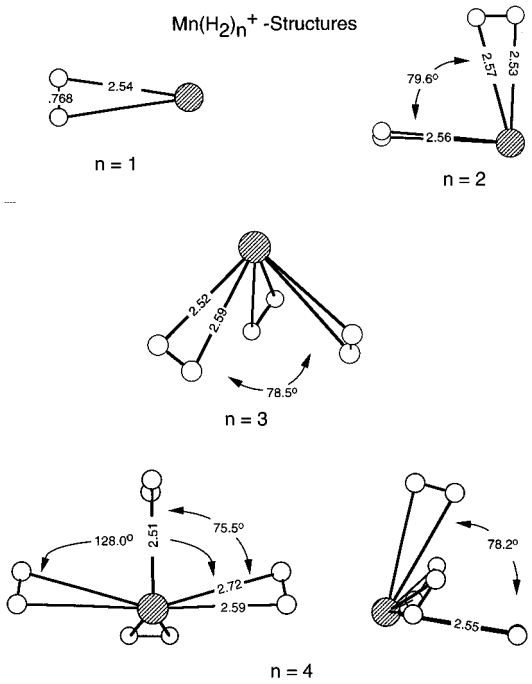

Figure 4. Calculated structures for $Mn^+(H_2)_n$, for $n = 1-4$; see text for details on method. All distances are in angstroms. The calculated H−H distance is 0.766 ± 0.001 Å. The two figures for $n = 4$ are related by a 90° rotation around the vertical axis in the plane of the paper.

TABLE 2: Natural Bond Order Populations on the Metal Center under Various Ligation Conditions

		population[a]		
	charge[a]	s	p	d
$Mn^+(H_2)$	0.971	+0.015	+0.010	+0.004
$Mn^+(H_2)_2$	0.949	+0.025	+0.020	+0.007
$Mn^+(H_2)_3$	0.933	+0.029	+0.028	+0.011
$Cr^+(H_2)$	0.987	+0.061	+0.007	−0.055
$Zn^+(H_2)$	0.946	+0.041	+0.016	−0.003
$Zn^+(H_2)_2$	0.912	+0.064	+0.029	−0.004
$Zn^+(H_2)_3$	0.892	+0.074	+0.039	−0.006
$Cu^+(H_2)$	0.984	+0.073	+0.010	−0.067

[a] The populations are calculated relative to the bare metal ion population. The s, p, and d populations refer primarily to 4s, 4p, and 3d orbital populations.

NBO populations (Table 2) show that there is about 1.5 times as much donation into the M^+ 4p orbitals in Mn^+H_2 and Zn^+H_2 as there is in Cr^+H_2 and Cu^+H_2 while donation into the Mn^+ and Zn^+ 4s orbitals is reduced (relative to Cr^+ and Cu^+). This use of the 4p orbitals is entirely analogous to the 3d/4s hybridization seen in most of the first-row M^+H_2 ions.[11,12] The Mn^+ ion in Mn^+H_2 also accepts a small amount of σ donation into the $3d\sigma$ orbital (Table 2), but the loss of d−d exchange energy makes this process even more unfavorable than donation into the 4s orbital. A spin change, leading to a $3d^6$ configuration can be ruled out since the lowest lying excited state (^5D) is 42 kcal/mol above the ground state.[16] The difference in the binding energy between Mn^+H_2 and Zn^+H_2 can almost certainly be attributed to the smaller size of the Zn^+ ion, which allows a closer approach and a stronger interaction with the H_2 molecule.[19]

$Mn^+(H_2)_2$ and $Zn^+(H_2)_2$. Our equilibrium data for $Mn^+(H_2)_2$ extend from 77 to 140 K and from 85 to 220 K for $Zn^+(H_2)_2$ (Figures 1 and 2). The experimental ΔH_T° and ΔS_T° values were −3.10 kcal/mol and −14.2 cal/(mol K) for Zn^+ and −1.9 kcal/mol and −11.7 cal/(mol K) for Mn^+ (Table 1). The theoretical structures are shown in Figures 3 and 4; the

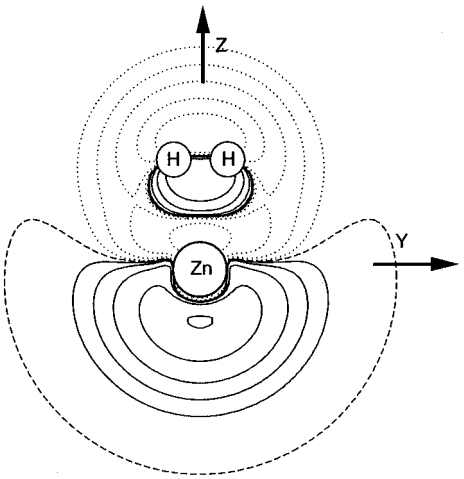

Figure 5. Differential density map of Zn^+H_2. The map is calculated as the total electron density distribution of Zn^+H_2 minus the densities of unperturbed Zn^+ and H_2, see text. Solid (dotted, dashed) lines represent increased (decreased, unchanged) electron density in Zn^+H_2 relative to the reactants. Note the significant increase in electron density opposite the Mn^+-H_2 bond, see text.

vibrational frequencies are listed in Table 3. There are no significant changes in the M^+-H bond lengths from the first cluster. From the usual analysis of the ΔG°_T vs T data, we obtain BDE's of 2.75 kcal/mol for $Zn^+(H_2)_2$ and 1.65 kcal/mol for $Mn^+(H_2)_2$. The calculated (DFT) BDE's are 3.10 kcal/mol for $Zn^+(H_2)_2$ and 1.56 kcal/mol for $Mn^+(H_2)_2$—in reasonable agreement with the experimental data. The rotation of the two H_2 units around their respective metal−ligand bond axes is essentially free. There are closely related structures that result from a 90° rotation of either one of the ligands (arranging the two H−H bonds parallel in space) which are higher in energy by only 0.07 kcal/mol.

Note that these BDE's are 1.00 and 0.25 kcal/mol *less* than the BDE's of the monomers. This is in strong contrast to most of the other transition metal hydrogen clusters[3,4,6,8,9,12,30] where the second H_2 ligand is significantly more strongly bound than the first. This typical increase in the BDE of the second H_2 might seem surprising since, by symmetry, the bonds are usually identical. The increase is due to the hybridization between the 3dσ orbital and the empty 4s orbital which is *already present* in the first cluster (to reduce Pauli repulsion on the bond axis). When the second H_2 is added, the cost of the hybridization is shared between two ligands, giving a larger BDE for the second H_2.[11,14] This effect has been predicted and observed in the first and second clusters of various transition metal ions with He, Ne, and Ar as well.[12] In $Mn^+(H_2)_2$ and $Zn^+(H_2)_2$, however, this 4s/3d hybridization is not beneficial due to the single occupancy of the 4s orbital and the filled 3d orbitals of Zn^+ and half-filled 3d shell of Mn^+. As a consequence, the second H_2 adds very much like the first. Again, the repulsive 4s electron density is polarized away from the H_2 ligand through partial hybridization with the $4p_x$ or $4p_y$ orbital. This results in near right angle geometries of $Mn^+(H_2)_2$ and $Zn^+(H_2)_2$. (The actual $H_2-M^+-H_2$ angles are 79.6° in Mn^+ and 91.3° in Zn^+ (see Figures 3 and 4).)

Most other first-row transition $M^+(H_2)_2$ complexes ($V^+(H_2)_2$,[3] $Cr^+(H_2)_2$,[4] $Fe^+(H_2)_2$,[5] $Co^+(H_2)_2$,[6,9] $Ni^+(H_2)_2$,[7] $Cu^+(H_2)_2$[8,30] have a 180° orientation due to the 4s/3d hybridization noted above.[11,12] The single exception is $Ti^+(H_2)_2$[2] which also has a 90° bent structure. In this case, however, the nonlinear geometry is due to the availability of two empty 3d orbitals to accept σ donation, and the ion makes little, if any, use of the 4p orbitals. The strongly bent geometry in the $Mn^+(H_2)_2$ and $Zn^+(H_2)_2$ ions, on the other hand, is a clear indication that the 4p orbitals are involved, since a filled or half-filled 3d valence shell is totally symmetric. The reduction in BDE's between the first and second H_2 ligands is very probably due to repulsion from the polarized electron cloud of the first H_2 ligand. Remember that 4p/4s partial hybridization moves a significant amount of electron density to the hemisphere of the M^+ opposite the H_2 ligand where it will increase the repulsion experienced by the second ligand. The differential population analyses clearly show a movement of the first cluster electron density distribution when the second H_2 is added, indicating that the ion attempts to reduce this repulsion. The reduction in BDE is far greater in $Zn^+(H_2)_2$ (26%) than in $Mn^+(H_2)_2$ (13%) due to the smaller size of the Zn^+ ion. The larger Mn^+ ion (and the longer Mn^+-H_2 bond lengths) also allow the H_2 ligands in $Mn^+(H_2)_2$ to avoid some of this repulsion by moving closer together (without increasing ligand−ligand repulsion). This may be the origin of the smaller bond angles in $Mn^+(H_2)_2$.

$Mn^+(H_2)_3$ and $Zn^+(H_2)_3$. Our data for the third clusters are shown in Figures 1 and 2. The experimental ΔH°_T and ΔS°_T values for Zn^+ are −2.58 kcal/mol and −15.2 cal/(mol K) (Table 1). Because of the very weak binding present in $Mn^+(H_2)_3$, we could obtain data only between 77 and 90 K. Due to the possibility of collision-induced dissociation after the cell, low cell pressures were required which in turn required very low temperatures to form a measurable amount of product. The end result was a temperature range too small to determine the slope of the ΔG°_T function. This precluded a direct measurement of ΔH°_T and ΔS°_T. To determine the ΔH°_0 for the third Mn^+ cluster, we used the dimer entropy and shifted it to match the third cluster data points (Figure 2, dashed line). This gave a BDE for $Mn^+(H_2)_3$ of 1.4 kcal/mol. The BDE of $Zn^+(H_2)_3$ was determined as usual (by fitting theoretical and experimental ΔG°_T vs temperature curves) and found to be 2.35 kcal/mol. The calculated values were 1.30 and 2.17 kcal/mol for $Mn^+(H_2)_3$ and $Zn^+(H_2)_3$, respectively.

The type of bonding seen in the first and second clusters continues here. Both $Mn^+(H_2)_3$ and $Zn^+(H_2)_3$ have structures with C_3-symmetry. The H_2 ligands again form angles of approximately 90° (78.2° in $Mn^+(H_2)_3$ and 86.5° in $Zn^+(H_2)_3$); i.e., the bond axes generally point in the x, y, and z directions. The bond lengths are all quite similar to those in the second cluster. In contrast, both $Cr^+(H_2)_3$[4] and $Cu^+(H_2)_3$[8] have very different planar structures with D_{3h} symmetry. In the case of $Mn^+(H_2)_3$ and $Zn^+(H_2)_3$ the geometry again reflects both the repulsive effect of the singly occupied 4s orbital and the ion's use of the 4p orbitals to polarize the 4s electron density away from the H_2 ligands, thereby reducing the σ repulsion and allowing a closer M^+-H_2 interaction. Each H_2 ligand interacts with one of the 4p orbitals and is thus oriented at approximately 90° to the others.

There is again a greater reduction in the BDE for Zn^+ than for the Mn^+. Again this must be due to the smaller size of the Zn^+ ion which forces the new ligand to interact more strongly with the polarized electron cloud. The smaller $H_2-M^+-H_2$ angle in the case of $Mn^+(H_2)_3$ (78.2°) can again be attributed to the larger size of the 4s orbital in $Mn^+(H_2)_3$, which allows the H_2 ligands to more closely approach each other in order to better avoid the electron density in the opposite hemisphere of the ion.

$Mn^+(H_2)_4$ and $Zn^+(H_2)_4$. Data for the fourth clusters is shown in Figures 1 and 2. Again, the very limited temperature range available for the Mn^+ system required us to scale the second cluster ΔG°_T function, giving a BDE of approximately 1.2 kcal/mol. This should probably be regarded as an upper

TABLE 3: Theoretical Vibrational Frequencies for Various $M^+(H_2)_n$ Clusters[a]

	H−H str[b]	asym M^+-H_2 str[b]	sym M^+-H_2 str[b]	$H_2-M^+-H_2$ bonds and rotations[b]
Mn^+H_2	4258	391	320	
$Mn^+(H_2)_2$	4270, 4266	400, 393	323, 314	149, 129, 114
$Mn^+(H_2)_3$	4272, 4271, 4271	406, 396, 396	315, 314, 304	171, 142, 137, 136, 123, 120
$Mn^+(H_2)_4$	4291, 4289, 4286, 4279	395, 394, 339, 328	310, 292, 278, 230	174, 158, 154, 143, 129, 122, 98, 88, 79
MnH^+				1729[c]
$MnH^+(H_2)$	4183	655	528	1778,[c] 159, 124
$MnH^+(H_2)_2$	4195, 4195	664, 662	501, 493	1789,[c] 227, 221, 171, 129, 102
Zn^+H_2	4172	498	482	
$Zn^+(H_2)_2$	4214, 4202	457, 454	420, 408	136, 104, 82
$Zn^+(H_2)_3$	4233, 4225, 4225	418, 418, 418	376, 355, 355	177, 152, 152, 124, 122, 122
$Zn^+(H_2)_4$	4257, 4250, 4249, 4244	404, 390, 328, 303	362, 338, 319, 244	204, 170, 169, 157, 141, 133, 130, 95, 87
$Zn^+(H_2)_5$	4282, 4275, 4275, 4260, 4257	360, 299, 288, 285, 283	346, 309, 276, 227, 219	212, 196, 163, 161, 152, 131, 125, 99, 96, 82, 71, 59
$Zn^+(H_2)_6$	4295, 4284, 4284, 4284, 4284, 4284	227, 227, 227, 220, 220, 220	312, 230, 230, 172, 172, 172	190, 160, 160, 160, 142, 142, 62, 62, 62, 61, 61, 61, 20, 19, 19
H_2	4365			
Cr^+H_2	4045	843	532	
Cu^+H_2	3796	1067	796	

[a] Harmonic vibrational frequencies for the different $M^+(H_2)_n$ clusters as obtained by analytical differentiation of the DFT (B3-LYP) energy. The distinction between the different types of low-frequency modes is increasingly artificial for the larger clusters. The frequencies for $Cr^+(H_2)$ and $Cu^+(H_2)$ are included for comparison. [b] All numbers in cm^{-1}. [c] Mn^+-H stretch frequency.

bound since, based on the $Zn^+(H_2)_4$ data, we expect a significant reduction in entropy (slope) for the fourth addition. The theoretical BDE was calculated to be 0.82 kcal/mol. The $Zn^+(H_2)_4$ data extended from 77 to 110 K, and the resulting ΔH_T° and ΔS_T° values were −1.81 kcal/mol and −12.6 cal/(mol K), respectively. The BDE ($-\Delta H_0^\circ$) from the theoretical fit to the data was 1.60 kcal/mol, and the value from theory was 1.2 kcal/mol. Structures of these fourth clusters are shown in Figures 3 and 4; the corresponding vibrations are listed in Table 3.

As can be seen from Figure 1 and Table 1, the BDE's of the different $Zn^+(H_2)_n$ clusters decrease in a stepwise manner with a strong reduction in stability at the tetramer. This is an obvious consequence of the use of the 4p orbitals in the bonding. In the first three clusters, three H_2 ligands interact with three separate partially hybridized 4p orbitals. In $Zn^+(H_2)_4$, however, one of the 4p orbitals must interact with two H_2 ligands. The calculated structures support this picture. Two H_2 ligands form an angle of approximately 180°, while the other angles are close to 90° (Figure 4). Because this pair of sp orbitals already has significant electron density, the resulting bond strength is reduced. This is consistent with the longer calculated Zn^+-H_2 bond lengths for the two opposed ligands.

Our calculations indicate that these arguments apply to the $Mn^+(H_2)_4$ cluster as well, although, as noted, the necessarily limited experimental data are not precise enough to confirm this. The calculated $Mn^+(H_2)_4$ structure does show the same features as $Zn^+(H_2)_4$. However, as in previous clusters, all the H_2-M-H_2 angles are somewhat smaller. This was the largest $Mn^+(H_2)_n$ cluster we could observe.

$Zn^+(H_2)_5$/$Zn^+(H_2)_6$. Limited data for the fifth Zn^+ cluster were taken between 77 and 90 K. The experimental ΔH_T° and ΔS_T° values were −1.6 kcal/mol and −13.5 cal/(mol K), respectively. The similarity of this entropy to those of the smaller clusters indicates that the first solvation shell is still being filled. The BDE of $Zn^+(H_2)_5$ is 1.50 kcal/mol, obtained by scaling the ΔG_T° function as described above for $Mn^+(H_2)_{3,4}$. The calculated BDE is 1.12 kcal/mol. The structure is a tetragonal pyramid (C_{2v} symmetry, Figure 3). This structure can easily be rationalized in terms of two partially hybridized 4p orbitals each interacting with two H_2 ligands, while one partially hybridized 4p orbital interacts with a single H_2. As expected, this axial H_2 is more strongly bound and has a shorter bond distance.

Data for $Zn^+(H_2)_6$ could be obtained only at 77 K. The single temperature point indicates that the BDE is slightly (0.1 kcal/mol) less strongly bound than the $Zn^+(H_2)_5$ cluster, i.e., that the BDE is about 1.4 kcal/mol. The calculated bond energy is 1.22 kcal/mol. The calculated structure for $Zn^+(H_2)_6$ is highly symmetric with T_h symmetry (Figure 3), but several isomers which result from rotation of the H_2 units around the $M-H_2$ bond axis are within 0.25 kcal/mol of the ground state. The BDE's of the last three H_2 ligands are equal within experimental uncertainty. This reflects the similarity of the bonding in the respective clusters.

$MnH^+(H_2)_n$. The addition of a single hydrogen atom to a manganese cation

$$Mn^+ + H_2 \rightarrow MnH^+ + H \qquad (3)$$

is endothermic for ground state manganese cations by ∼50 kcal/mol, due to the high dissociation energy of H_2 (104 kcal/mol) compared to 53 kcal/mol[38] for the BDE of MnH^+. Nevertheless, we observe MnH^+ and $MnH^+(H_2)_n$ clusters with a total intensity of 5−10% of the $Mn^+(H_2)_n$ clusters. This is about the same ratio we observe from the ESC data for the excited state Mn^+ ($3d^6$ configuration) vs ground state Mn^+ ($3d^54s$ configuration). It is therefore very likely that the observed $MnH^+(H_2)_n$ clusters are formed by the reaction of the excited state manganese with hydrogen. This reaction is also driven by the translational deexcitation of Mn^+ ions as they enter the reaction cell. The injection energy can be adjusted to several hundred electronvolts to maximize production of these higher energy species. The ionic product is ground state $^6\Sigma$ MnH^+, which subsequently clusters with one or more H_2 ligands. Equilibria for these ions were investigated in exactly the same way as for the simple $M^+(H_2)_n$ clusters. Data are shown in Figure 2.

$MnH^+(H_2)$. Equilibrium data for the $MnH^+(H_2)/MnH^+$ system were taken in the range between 220 and 400 K. The experimental ΔH_T° and ΔS_T° values were −7.58 kcal/mol and −18.0 cal/(mol K). The fitting procedure gave a BDE of 7.15 kcal/mol, in excellent agreement with the calculated value of 7.26 kcal/mol. This is more than 3 times the BDE of Mn^+H_2 and is quite similar to that of Cr^+H_2.[4] The large increase in

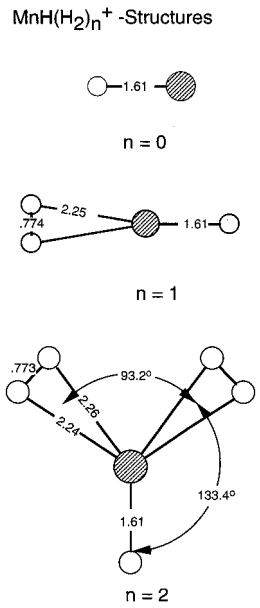

Figure 6. Calculated structures for MnH^+, $MnH^+(H_2)$, and $MnH^+(H_2)_2$; see text for details on method. All distances are in angstroms.

BDE can be attributed to formation of a localized, highly directional Mn^+-H σ bond from the hydrogen 1s electron and the diffuse, repulsive 4s electron in bare Mn^+. Formation of this bond removes the long-range repulsion experienced by the H_2 ligand in Mn^+H_2, and MnH^+ behaves as a $3d^54s^0$ ion very similar to Cr^+H_2.

$MnH^+(H_2)_2$. The data set for $MnH^+(H_2)_2$ extend from 150 to 300 K; the experimental ΔH_T° and ΔS_T° values were -5.33 kcal/mol and -17.6 cal/(mol K). The optimum ΔG_T° fit gives a BDE of 4.8 ± 0.5 kcal/mol. This energy is in excellent agreement with the DFT calculations which predict 4.74 kcal/mol for this bond strength. The second H_2 ligand in $Cr^+(H_2)_2$ is bound by 8.95 kcal/mol—almost twice as strongly as in $MnH^+(H_2)_2$. This difference can be understood in terms of the different geometries of $MnH^+(H_2)_2$ and $Cr^+(H_2)_2$ (Figure 6). In the chromium cluster, the H_2 ligands bind opposite to one another, leading to a D_{2d} geometry in which the cost of s/d hybridization is shared between the two H_2 ligands. The structure is also very favorable in terms of back-donation (although this is a small effect in $Cr^+(H_2)_2$). Such a geometry is not possible in $MnH^+(H_2)_2$ since the covalently bound hydrogen atom occupies one site and the two H_2 ligands are forced into a less favorable C_{2v} orientation. It should be noted the BDE of $MnH^+(H_2)_2$ is very similar to that of $Cr^+(H_2)_3$, however (4.70 kcal/mol), which has a structure nearly identical to $MnH^+(H_2)_2$. This result further supports the assignments of a $3d^54s^0$ electronic configuration to Mn^+ in the MnH^+ core moiety.

Conclusions

1. Binding energies have been measured for the first six $Zn^+(H_2)_n$ cluster ions as well as the first four $Mn^+(H_2)_n$ cluster ions. The Zn^+ binding energies are (in order of cluster size) 3.75, 2.75, 2.35, 1.60, 1.50, and ~1.4 kcal/mol. The corresponding Mn^+-H_2 BDE's are 1.90, 1.65, ~1.4, and ~1.2 kcal/mol.

2. Density functional calculations (B3-LYP parametrization) were done on all the ions to obtain theoretical BDE's, geometries, and vibrational frequencies. Agreement between the theoretical and experimental BDE's is in all cases good, usually within the experimental uncertainty (Table 1).

3. These energies are by far the weakest among the first-row transition metals. This is due primarily to the presence of a 4s valence electron in these ions and, to a lesser extent, to the presence of filled and half-filled 3d shells. The ground state of Mn^+ is ^7S ($[Ar]3d^54s^1$), and that of Zn^+ is ^2S ($[Ar]3d^{10}4s^1$). All other first-row transition metals, by contrast, assume a $3d^n$ valence electron configuration in the $M^+(H_2)_n$ clusters. In these cases, the 4s orbital does not produce Pauli repulsion along the bond axis and can accept electron density from the ligands. When the 4s is occupied, these effects are reversed, and the result is the greatly diminished BDE's we observe. The large 3d exchange stabilization energy in Mn^+ and the closed shell in Zn^+ may also lead to reduced amounts of M^+ $3d\pi$ to H_2 σ^* back-donation which further weakens the M^+-H_2 bond. This effect is difficult to separate from the reduction due simply to the longer bond distances induced by the occupied 4s orbital, however.

4. Although Mn^+ and Zn^+ are symmetric ions (^7S and ^2S), their $M^+(H_2)_n$ clusters are not: The H_2 ligands for $n = 2-6$ form angles ($H_2-M^+-H_2$) of approximately 90° with each other. This can be rationalized in terms of (a) the repulsive effect of the half-filled 4s orbital and (b) partial hybridization of the 4p orbitals with the 4s orbital to form hybrid sp orbitals that both accept electron density from H_2-M^+ donation and move the 4s electron density away from the H_2 ligand.

5. We have also determined bond energies for $MnH^+(H_2)$ and $MnH^+(H_2)_2$ (4.80 and 7.15 kcal/mol). These bond energies are more than 3 times higher than those of the corresponding clusters of a pure manganese cation. The reason for this increase lies in the highly directed bonding of the metal ion's singly occupied 4s orbital with the hydrogen 1s orbital. This makes the MnH^+ molecular ion a quasi-$3d^5$ transition metal with bond energies comparable to the chromium cation.

Acknowledgment. The support of the National Science Foundation under Grant CHE-9421126 is gratefully acknowledged. P. Weis thanks the "Deutscher Akademischer Austauschdienst" for financial support.

References and Notes

(1) Bushnell, J.; Kemper, P. R.; Maître, P.; Bowers, M. T. *J. Am.Chem. Soc.* **1994**, *116*, 9710.
(2) Bushnell, J.; Kemper, P. R.; Bowers, M. T. To be submitted.
(3) Bushnell, J.; Kemper, P. R.; Bowers, M. T. *J. Phys. Chem.* **1993**, *97*, 11628.
(4) Kemper, P. R.; Weis, P.; Bowers, M. T. *Int. J. Mass Spectrom. Ion Processes*, in press.
(5) Bushnell, J.; Kemper, P. R.; Bowers, M. T. *J. Phys. Chem.* **1995**, *99*, 15602.
(6) Kemper, P. R.; Bushnell, J.; von Helden, G.; Bowers, M. T. *J. Phys. Chem.* **1993**, *97*, 52.
(7) Kemper, P. R.; Weis, P.; Bowers, M. T. To be submitted.
(8) Kemper, P. R.; Weis, P.; Maître, P.; Bowers, M. T. To be submitted.
(9) Kemper, P. R.; Bushnell, J.; van Koppen, P. A. M.; Bowers, M. T. *J. Phys. Chem.* **1993**, *97*, 1810.
(10) van Koppen, P. A. M.; Bushnell, J.; Kemper, P. R.; Bowers, M. T. *J. Am. Chem. Soc.* **1995**, *117*, 2098.
(11) Bauschlicher, C. W.; Partridge, H.; Langhoff, S. R. In *Organometallic Ion Chemistry*; Freiser, B. S., Ed.; Kluwer Academic: Dordrecht, The Netherlands, 1996.
(12) (a) Bauschlicher, C. W.; Partridge, H.; Langhoff, S. R. *J. Chem. Phys.* **1989**, *91*, 4733. (b) Partridge, H.; Bauschlicher, C. W.; Langhoff, S. R. *J. Phys. Chem.* **1992**, *96*, 5350. (c) Bauschlicher, C. W.; Partridge, H.; Langhoff, S. R. *Chem. Phys. Lett.* **1990**, *165*, 272.
(13) Maître, P.; Bauschlicher, C. W. *J. Phys. Chem.* **1995**, *99*, 6836.
(14) Bauschlicher, C. W.; Maitre, P. *J. Phys. Chem.* **1995**, *99*, 3444.
(15) Perry, J. K.; Ohanissian, G.; Goddard, W. A. *J. Phys. Chem.* **1993**, *97*, 5238.
(16) Moore, C. E. *Atomic Energy Levels*; *Natl. Bur. Stand.* (*U.S.*) Circ. 1949, No. 467.
(17) Kubas, G. J.; Ryan, R. R.; Swanson, B. I.; Vergamini, P. J.; Wasserman, H. J. *J. Am. Chem. Soc.* **1984**, *106*, 451.
(18) Weisshaar, J. C. *Acc. Chem. Res.* **1993**, *26*, 213.

(19) (a) Barnes, L. A.; Rosi, M.; Bauschlicher, C. W. *J. Chem. Phys.* **1990**, *93*, 609. (b) Desclaux, P. *At. Data Nucl. Data Tables* **1973**, *12*, 312.
(20) Kemper, P. R.; Bowers, M. T. *J. Am. Soc. Mass Spectrom.* **1990**, *1*, 197.
(21) Type 615, 100 Torr; MKS Inc., Andover, MA 01810.
(22) ACE MCS; EG&G Ortec, Oak Ridge, TN 37830.
(23) Kemper, P. R.; Bowers, M. T. *J. Phys. Chem.* **1991**, *95*, 5134. Bowers, M. T.; Kemper, P. R.; von Helden, G.; van Koppen, P. A. M. *Science* **1993**, *260*, 1446.
(24) Hohenberg, P.; Kohn, W. *Phys. Rev. B* **1964**, *136*, 864.
(25) Kohn, W.; Sham, L. J. *Phys. Rev. A* **1965**, *140*, 1133.
(26) Becke, A. D. *J. Chem. Phys.* **1993**, *98*, 5648.
(27) Becke, A. D. *Phys. Rev. A* **1988**, *38*, 3098.
(28) Lee, C.; Yang, W.; Parr, R. G. *Phys. Rev. B* **1988**, *37*, 785.
(29) Vosko, S. H.; Wilk, L., Nusair, M. *Can. J. Phys.* **1980**, *58*, 1200.
(30) Maître, P.; Bauschlicher, C. W. *J. Phys. Chem.* **1993**, *97*, 11912.
(31) Maître, P.; Bauschlicher, C. W. *J. Phys. Chem.* **1995**, *99*, 6836.
(32) Ahlrichs, R.; Bär, M.; Häser, M.; Horn, H.; Kölmel, C. *Chem. Phys. Lett.* **1989**, *162*, 165.
(33) Treutler, O.; Ahlrichs, R. *J. Chem. Phys.* **1995**, *102*, 346.
(34) Frisch, M. J.; Trucles, G. W.; Head-Gordon, M.; Raplogle, E. S.; Gomperts, R.; Andres, J. L.; Raghavachari, K.; Binkley, J. S.; Gonzales, C.; Martin, R. L.; Fox, D. J.; Defrees, D. J.; Baker, J.; Stewart, J. J. P.; Pople, J. A. *Gaussian 92*; Gaussian Inc.: Pittsburgh, PA, 1993.
(35) Schäfer, A.; Horn, H.; Ahlrichs, R. *J. Chem. Phys.* **1992**, *97*, 2571.
(36) Bushnell, J.; Kemper, P. R.; Bowers, M. T. *J. Phys. Chem.* **1994**, *98*, 2044.
(37) Reed, A. E.; Curtis, L. A.; Weinhold, F. *Chem. Rev.* **1988**, *88*, 899 and references therein.
(38) (a) Carter, E. A.; Goddard, W. A. *J. Phys. Chem.* **1988**, *92*, 5679. (b) Stevens, A. E.; Beauchamp, J. L. *Chem. Phys. Lett.* **1981**, *78*, 291. (c) Elkind, J. L.; Armentrout, P. B. *J. Chem. Phys.* **1986**, *84*, 4862.